On the polarization of oscillatory currents in the Bay of Biscay

Hans van Haren
Royal Netherlands Institute for Sea Research (NIOZ), Den Burg, Netherlands

Received 4 December 2002; revised 6 May 2003; accepted 15 May 2003; published 10 September 2003.

[1] Rotary spectral properties were examined using ~20 records of yearlong current observations in the Bay of Biscay. Here data are discussed from two representative records from 1000 m above the bottom at two sites, one above the continental slope and another above the abyssal plain. Nearly raw spectra revealed a strong prevalence for clockwise over anti-clockwise circular motions at frequencies (σ) between $\sim 0.85f < \sigma < N$ (f and N denoting the local inertial and buoyancy frequencies, respectively). The observations showed rotary properties that were previously associated with free internal waves (for $f < \sigma < N$, $N \gg f$), but only for motions in bands of ~0.9 cpd width in frequency around inertial, tidal, and their nonlinear sum-interaction frequencies. This width was larger than the enhanced kinetic energy bands of ~0.15 cpd around inertial and tidal constituent frequencies. Nevertheless, it was suggested that both bands were associated with the same nonlinear interactions due to advection between subinertial and peak-frequency motions that also resulted in internal wave intermittency. *INDEX TERMS:* 4544 Oceanography: Physical: Internal and inertial waves; 4512 Oceanography: Physical: Currents; 4560 Oceanography: Physical: Surface waves and tides (1255); 4594 Oceanography: Physical: Instruments and techniques; *KEYWORDS:* Bay of Biscay, currents, internal waves, polarization

Citation: van Haren, H., On the polarization of oscillatory currents in the Bay of Biscay, *J. Geophys. Res.*, *108*(C9), 3290, doi:10.1029/2002JC001736, 2003.

1. Introduction

[2] The rotation of the Earth has major impact on motions in the ocean. This is evident from the equations of motion for horizontal (oscillatory) current components (u, v) in a Cartesian coordinate system (x, y),

$$\begin{aligned} \frac{\partial u}{\partial t} &= fv + \pi_x + \delta_x - \xi_x + B_x, \\ \frac{\partial v}{\partial t} &= -fu + \pi_y + \delta_y - \xi_y + B_y, \end{aligned} \tag{1}$$

where the Coriolis terms (fv, $-$fu) describe an apparent force dependent on the inertial frequency $f = 2\Omega\sin\varphi$, twice the local vertical component of the Earth's rotation vector $\mathbf{\Omega}$ at latitude φ. The B indicate external body forces. The π, δ, and ξ schematically indicate perturbation terms representing pressure gradient, diffusive fluxes, and nonlinear advection, respectively. *Ekman* [1905] explored the inertial-stress balance for frictional boundary layers, "Ekman dynamics." Important improvements in data analyses of near-surface horizontal oscillatory currents in a rotating (f-) frame of reference were made by *Gonella* [1972], who introduced "rotary spectra."

[3] In this paper, some of Gonella's methods are used to study deep-ocean motions well away from boundaries, specifically those from the "internal wave" frequency (σ) band $f < \sigma < N$ ($N \gg f$, N the buoyancy frequency). Previously, such methods have been applied to relatively strongly smoothed spectra by *Müller et al.* [1978] and *Fu* [1981]. Applying consistency tests, *Müller et al.* [1978] demonstrated that open ocean (Sargasso Sea) current spectra from 42 days of data were featureless and well characterized by random linear internal waves between $f < \sigma < \sim 20$ cycles per day. Here varyingly smoothed spectra of yearlong current measurements are used from two sites over the continental slope in the Bay of Biscay. Recent observations [*Mihaly et al.*, 1998; *van Haren et al.*, 1999, 2002] and numerical modeling work [*Xing and Davies*, 2002] show that the internal wave band can be dominated by strong nonlinear (advection) interactions between near-inertial and semidiurnal tidal motions. Such observations of strong nonresonant nonlinear interactions follow theoretical suggestions [*Phillips*, 1977] and are in contrast with weak resonant ("wave-wave") interaction models [*Müller et al.*, 1986]. Thus the focus here is on the use of rotary spectral properties to distinguish between barotropic and baroclinic motions, free propagating internal waves, nonlinearly forced motions, and fine structure contamination. Such distinction is not possible or difficult using kinetic energy spectra.

2. Rotary Components and Spectra

[4] *Gonella* [1972] analyzed circular rotary current components,

Anti-clockwise rotary component

$$w_+ = \frac{\tilde{u} - i\tilde{v}}{2} = W_+ \exp(-i\theta_+) \tag{2a}$$

Clockwise rotary component

$$w_- = \frac{\tilde{u} + i\tilde{v}}{2} = W_- \exp(i\theta_-), \tag{2b}$$

0148-0227/03/2002JC001736$09.00

for harmonic $\tilde{u} = U \exp(i\varphi_u)$ and similarly for $\tilde{v}$, which combines oscillatory current components $(u, v) = \mathrm{Re}(\tilde{u}\exp(-i\sigma t), \tilde{v}\exp(-i\sigma t)) = (U\cos(\sigma t - \varphi_u), V\cos(\sigma t - \varphi_v))$ into one complex current,

$$w = u + iv = w_+^* \exp(i\sigma t) + w_- \exp(-i\sigma t), \quad (3)$$

where ()* denotes a complex conjugate, $i^2 = -1$ and σ is the harmonic frequency. Any horizontal current ellipse is a sum of the two rotary components (equation (2)), so that a rectilinear oscillatory motion is composed of rotary components having equal amplitudes.

[5] *Gonella* [1972] focused on spectral properties of the rotary components to learn more about the relation between wind stress and near-surface ocean currents in terms of Ekman dynamics. Rotary amplitude spectra are defined,

Anti-clockwise spectrum

$$P_+(\sigma) = \langle w_+ \rangle^* \langle w_+ \rangle / 2 \quad (4a)$$

Clockwise spectrum

$$P_-(\sigma) = \langle w_- \rangle^* \langle w_- \rangle / 2, \quad (4b)$$

where the brackets denote the Fourier transform, so that the kinetic energy spectrum is their sum,

$$P_{KE}(\sigma) = P_-(\sigma) + P_+(\sigma). \quad (5)$$

The difference between the rotary spectra (equation (4)) is a measure for the polarization, for which *Gonella* [1972] introduced the "rotary coefficient,"

$$C_R(\sigma) \equiv (P_-(\sigma) - P_+(\sigma))/P_{KE}(\sigma), \quad (6)$$

where C_R is equal to zero for purely rectilinear motion and equal to ± 1 for purely circular motion. Its sign indicates the direction in which the ellipse is traversed, clockwise or anti-clockwise. Under linear perturbation and neglecting frictional stresses, so that $\delta = \xi = 0$ in equation (1), the (free internal wave) solution of equation (6) becomes

$$|C_R(\sigma)| = \frac{|W_-^2 - W_+^2|}{W_-^2 + W_+^2} = \frac{2\sigma f}{\sigma^2 + f^2}, \quad \text{when } |\pi_+| = |\pi_-|, \quad (7)$$

the forcing being independent of the sense of rotation: "symmetric forcing" [*Gonella*, 1972]. This implies forcing in one Cartesian direction only: for example $\pi_x = 0$, or $\pi_y = 0$. For asymmetric forcing the model for C_R is no longer sign independent and it becomes more complicated due to the dependence on the (different) rotary forcing components.

[6] Comparing observations with the above theory, *Gonella* [1972] found a strong asymmetry in C_R around f, in reasonable agreement with equation (7) for $f < \sigma < N$ and showing much lower values than equation (7) for $\sigma < f$. At these subinertial frequencies, anti-clockwise forcing was apparently much larger than clockwise forcing. *Gonella* [1972] attributed this disagreement between theory and observations to nonpropagating clockwise motions for $\sigma < f$. Note that he did not consider nonlinear forcing.

[7] A different spectral property, providing similar ellipse information as C_R, was examined by *Fu* [1981],

$$A_R(\sigma) \equiv \frac{P_-(\sigma)}{P_+(\sigma)} = \frac{(\sigma + f)^2}{(\sigma - f)^2}, \quad (8)$$

for linear internal waves; $A_R(f) \gg 1$ implies dominance of the clockwise rotary near-inertial motion. This dominance of clockwise over anti-clockwise motions decreases with increasing frequency in the internal wave band, as in equation (7). Like *Gonella* [1972], *Fu* [1981] also observed $A_R(\sigma) > 1$ for subinertial frequencies $(0.4-0.6)f < \sigma < f$, and a weak dominance of anti-clockwise motions ($A_R(\sigma) < 1$) for $0.05f < \sigma < 0.4f$. Fu suggested nonlinear interactions between inertial waves and low-frequency motions to explain these observations at subinertial frequencies. In the present paper, observations are compared with equations (7) and (8) and A_R is used for graphs.

3. Data

[8] Currents were evaluated from measurements at two moorings at 46°39′N, 05°29′W (BB3; H_A = 2450 m water depth) and at 45°48′N, 06°50′W (BB8; H_B = 4810 m) in the Bay of Biscay (Figure 1). The moorings consisted of four Aanderaa RCM-8 current meters (at 50, 300, 600, and 1000 m above the bottom), sampling at once per 20 min for 11 months, below a single buoyancy package. Here the focus is on data from the upper instruments, at 1000 m above the bottom, to avoid any possible bottom boundary layer effects. The kinetic energy spectra of these observations (Figure 2) are typical examples representative of all records from the eight moorings (BB1 through BB8) that were deployed down the continental slope and out into the abyssal plain. Above the steep bottom slope (>10° in places), tidal currents dominated (e.g., BB3, also representing BB1–BB6 except BB5), while above the abyssal plain, near-inertial motions were relatively more important (e.g., BB8, also representing BB5, BB7).

[9] At BB3 and BB8, maximum currents were 0.33 and 0.14 m s^{-1}, respectively. At both moorings, the current speeds were comparable over the entire mooring line of 1000 m length. The pressure sensors at the uppermost current meters did not vary by more than 2 digits (∼12 dbar) over the entire record. As a result, mooring motions generated negligibly small artificial spectral peaks at (nonlinear inertial-tidal) frequencies.

[10] In the spectral analysis variable smoothing is applied, $\nu \approx 3-40$ degrees of freedom (dof). Only a tapered time series is used without further smoothing ($\nu \approx 3$ dof, yielding a (equivalent) bandwidth of ∼0.007 cpd for an 11-month record), regarding some (e.g., tidal) motions deterministic rather than a particular realization of a (random) stochastic process. For the entire record, the smoothing $\nu \approx 3$ dof is applied for $\sigma < 0.1$ cpd, $\nu \approx 15$ dof for $0.1 < \sigma < 3.1$ cpd, and $\nu \approx 30$ dof for $\sigma > 3.1$ cpd.

[11] CTD-profiles were obtained within 4 km from each mooring just before their recovery. These profiles were used to estimate "background" stratification. At z = −1500 m $N_A = 28 \pm 15$ cpd for mooring BB3, at z = −3800 m N_B =

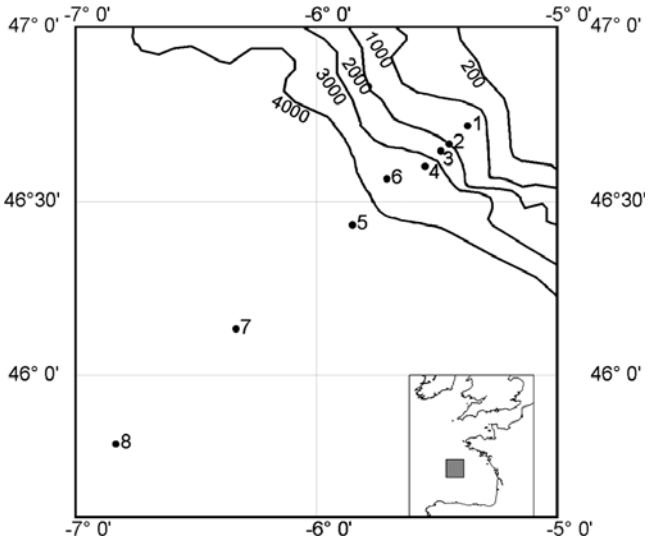

Figure 1. Map of the Bay of Biscay (BB), with mooring numbers indicated.

7 ± 4 cpd for mooring BB8. Frequency was calculated in cycles per day (1 cpd = $2\pi/86400$ s^{-1}).

4. Observations

[12] The kinetic energy spectra did not just show significant peaks at semidiurnal tidal and near-inertial frequencies (Figure 2). Within the internal wave band, significant peaks were also observed at higher tidal harmonic frequencies, but especially also at sum-interaction frequencies involving f and tidal harmonics, for example $M_2 + f$, $M_4 + f$, …, M_4, M_6, … [*van Haren et al.*, 2002]. (In Figure 2, only components are displayed associated with lunar M_2, but nearly raw spectra also showed harmonics associated with tidal constituents S_2, N_2, L_2, …. The semidiurnal band D_2, defined between $0.9M_2 < \sigma < 1.1M_2$, was represented by dominant M_2.) The rotary spectral observations provide additional information on these internal wave band peaks.

[13] The observed yearlong average $A_R(\sigma)$ (Figure 3) and $C_R(\sigma)$ (not shown) showed the familiar strong dominance of clockwise motions near the inertial frequency.

[14] Within the internal wave band, A_R decreased with increasing frequency, as predicted by equation (8). In detail, the observations did not show a smooth decrease with frequency. Instead, they showed some significant elevated bands ("peaks") and depressed bands ("gaps"). Within D_2, current ellipses at lunar tidal M_2 varied from almost rectilinear (a relatively small $A_R(M_2)$) above the abyssal plain (Figure 3a) to predominantly clockwise circular above the continental slope (Figure 3b). This implied dominant barotropic M_2 at BB8, and it suggested, possibly, (large-scale, yearlong persisting) baroclinic M_2 at BB3. At both sites, motions at solar S_2 were strongly clockwise circular and hence, possibly, (large-scale) baroclinic. It is noted that baroclinic tidal motions have a specific polarization according to equations (7) and (8), while barotropic motions can attain all polarization, depending on basin shape and other topographic effects. Above details at M_2 and S_2 were also observed in nearly raw rotary spectra (equation (4)) (Figure 4).

[15] This detail of the fSD band, defined between $0.9f < \sigma < 1.1S_2$, showed the aforementioned differences at M_2

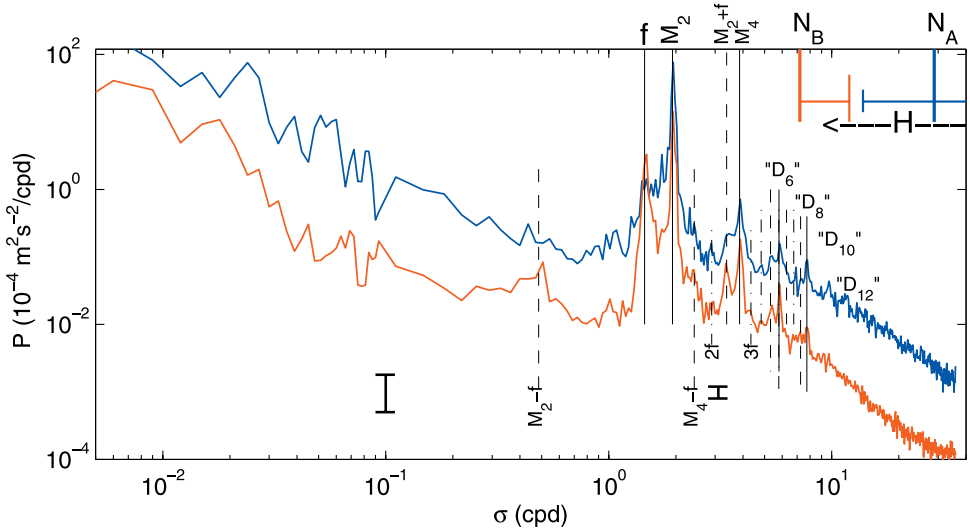

Figure 2. Varyingly smoothed kinetic energy spectra from 11 months current meter observations at z = −3810 m (mooring BB8; red spectrum; $P_B(\sigma)$) and at z = −1450 m (BB3; blue spectrum $P_A(\sigma)$). The smoothing is for $\nu \approx 3$ degrees of freedom (dof; ∼raw), $\nu \approx 15$ dof, $\nu \approx 30$ dof. The latter two are used to compute the 95% significance intervals, valid to the right of their position on the frequency axis. The spectra are not deliberately offset vertically, and their vertical shift in energy contents reflects the difference in stratification (N) and water depth (H), see upper right. Note that near-inertial energy is larger at BB8 than at BB3. Several spectral lines are indicated, individually and in bands (indicated between double quotes, D meaning "diurnal").

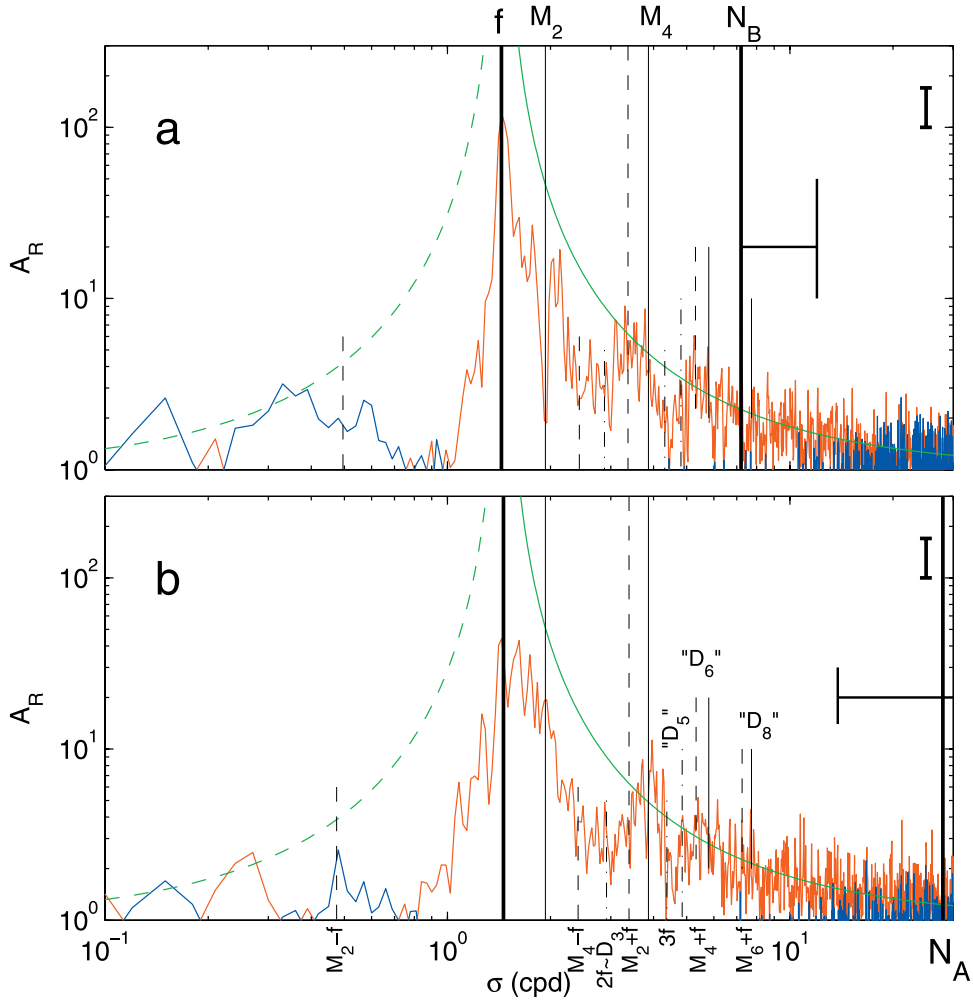

Figure 3. Moderately smoothed ($\nu \approx 30$ dof) rotary energy ratio compared with linear (internal wave) model (equation (8)), indicated by the smooth green curve that is dashed for $\sigma < f$ where it is formally not applicable. $A_R(\sigma)$ is indicated in red when $P_-(\sigma) > P_+(\sigma)$ and in blue otherwise. (a) Observations at $z = -3810$ m (BB8). (b) Observations at $z = -1450$ m (BB3).

between the two sites, which more or less also existed at less energetic tidal constituents like μ_2, N_2, and L_2. More importantly, the nearly raw spectra showed the clockwise dominance at nearly all frequencies within the fSD band, also at frequencies not labeled with known tidal constituents. This implied stable estimates (as opposed to random noise) at these "unlabeled" frequencies. These observations suggested nonlinear interaction between peak-frequency motions (like at f and M_2) with varying background conditions, namely, low-frequency stratification and current variations, as will be discussed in section 5. An indication for a relationship between stratification and kinetic energy levels was the observed N-scaling of the spectra: power $P(\sigma) \sim N\sigma^{-2}$, which not only applied for the internal wave band interior ($f \ll \sigma \ll N$ [*Garrett and Munk*, 1972]), but also between f and D_2 (Figure 2). This was inferred from the ratio between the two spectra $P_B/P_A \sim N_B/N_A$, which remained constant for $\sim 1.1f < \sigma < N_B$, except for inertial-tidal interaction bands.

[16] Despite the observed N-scaling between the two data sets, only peaks in A_R concurred with the linear internal wave predictions (equation (8)), more or less up to $\sigma = N$ (Figure 3). For $\sigma > D_2$, the peaks in A_R were centered at sum-tidal-inertial interaction frequencies (like $M_2 + f$, $M_4 + f$) in record BB8 when the kinetic energy ratio $P_{KE}(f)/P_{KE}(M_2)$ was large (Figure 3a) and at even higher tidal harmonics (like M_4 and M_6) in record BB3 when this ratio was relatively low (Figure 3b). Both sites exhibited local minima in A_R in frequency bands including difference-interaction frequencies like $M_4 - f$, $S_4 - f$, $N_4 - f$, ..., $M_6 - f$, $S_6 - f$, $N_6 - f$, but also 2f, 3f, and odd tidal harmonics like in D_3 (M_3, S_3, N_3, ...) with notable exception the band D_5. Neglecting gaps at individual frequencies like at M_2 (Figure 3a), peaks (and gaps) in A_R occurred in frequency bands of approximately constant width $\Delta\sigma = 0.9 \pm 0.1$ cpd (note log scale in Figure 3). As a result, relatively dominant clockwise motions were found in a band from 0.9f to $1.1S_2$, but also in bands grouping together $D_2 + f$ and D_4, and the D_6 band. These bands were distinct in the kinetic energy spectra (Figure 2), but with separate peaks at individual frequencies like $M_2 + f$ and M_4. Such peaks were absent in A_R. This property of

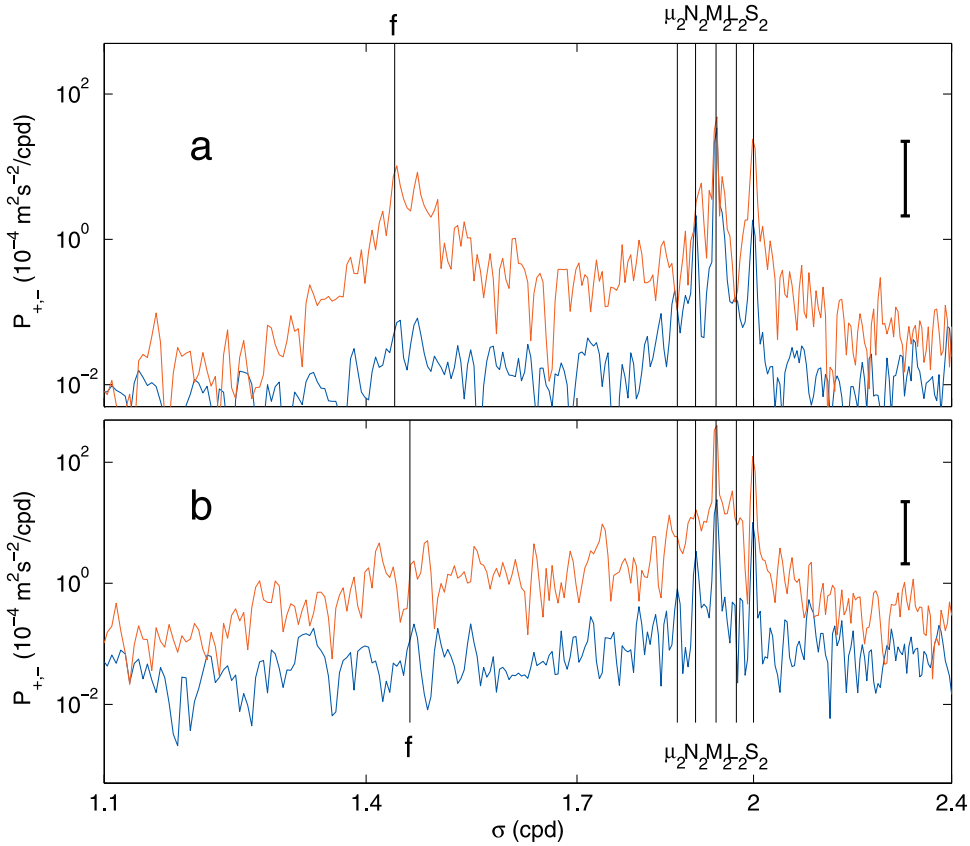

Figure 4. Near-raw rotary spectral details of the fSD band. The weak smoothing ($\nu \approx 3$ dof) was achieved by using just a single Kaiser window taper over the entire time series. Clockwise rotary spectrum is in red, anti-clockwise in blue. (a) Observations at $z = -3810$ m (BB8). (b) Observations at $z = -1450$ m (BB3).

A_R (and C_R) was used to express the significantly different bands of sum- and difference-tidal-inertial interaction frequencies in one ratio, which was about constant (c),

$$\frac{C_R(M_2+f)}{C_R(M_2-f)} \approx \frac{C_R(M_4+f)}{C_R(M_4-f)} \approx c \approx 2,$$

$$\frac{A_R(M_2+f)}{B_R(M_2-f)} \approx \frac{A_R(M_4+f)}{B_R(M_4-f)} \approx c \approx 2, \qquad (9)$$

$$B_R = A_R \text{ for } P_-(\sigma) > P_+(\sigma), \text{and}$$

$$B_R = A_R^{-1} \text{ for } P_-(\sigma) < P_+(\sigma).$$

For $n > 2$ the observed bands were not significantly different in a (random) statistical sense. A maximum ratio $A_R/B_R \approx 4$ was found for $M_2 + f$ and $M_2 - f$ at BB8 (Figure 3a). Below, the implications of $c > 1$ will be discussed.

5. Discussion

[17] The observed $A_R(\sigma)$ yielded additional information on internal wave motions compared to kinetic energy spectra. This information is interpreted as follows.

[18] With reference to equation (1), the correspondence between A_R and the observations at sum-tidal-inertial and even tidal harmonic interaction frequencies implied symmetric nonlinear advection forcing $|\xi_+| = |\xi_-|$. Such forcing may have been imposed by the local or continental slope topography. As no linear forcing at these sum-interaction frequencies is known, equation (8) is also valid for symmetric nonlinear forcing. The differences between model and observations suggested that in other (e.g., difference-interaction) frequency bands the forcing was asymmetric. In these bands, relatively less energetic motions were found.

[19] Additionally, the A_R, and more clearly the ratio equation (9), provided a means for discriminating between dynamic and kinematic (finestructure contamination) effects in moored observations, as explained below. As an example of the latter, if a phase-locked signal at $M_2 + f$ was perfectly clockwise circular ($A_R \rightarrow \infty$), that at $M_2 - f$ should be perfectly anti-clockwise ($A_R \rightarrow 0$), with both rotary amplitudes being equal and $c = 1$. This example followed from a kinematic (vertical) advection model of a plane inertial wave propagating through a (standing) sinusoidal wave field and observed in a Eulerian frame of reference [*Alford*, 2001]. Our observed ratios $c > 1$ in equation (9) expressed the dominance of plane over standing wave motions during nonlinear interactions; this suggested dynamics were more important than kinematics. Such importance was also suggested in modeling results of *Xing and Davies* [2002]. Unfortunately, the A_R or A_R/B_R ratio could not discriminate

unambiguously between free- and phase-locked nonlinear waves, unless the above kinematic model was the only reason for observing phase-locked motions. However, there may be another reason, suggested below.

[20] Principally, freely propagating internal plane waves cannot result from nonlinear advective terms ξ in equation (1), because such waves supported by continuous stratification and propagating in an unbounded ray have the property,

$$\mathbf{u} \cdot \mathbf{k} \equiv 0, \tag{10}$$

for current and wave number vectors **u** (in the plane of group speed $\mathbf{c_g}$) and **k** (in the plane of phase speed $\mathbf{c} \perp \mathbf{c_g}$), respectively, so that nonlinear terms disappear from the equations for vorticity and buoyancy [*LeBlond and Mysak*, 1978]. In contrast, in a wave ray of finite spatial extent, a wave "group," nonlinear (advection) terms do not vanish from the governing equations.

[21] Suggested evidence of internal wave groups were the observed enhanced spectral bands of finite extent in frequency, being wider than single sharp deterministic harmonics and narrower than the entire internal wave band. Such enhanced spectral bands had a typical width of $\sim$0.1–0.2 cpd around frequencies like f in A_R and around f and, for example, M_2 in the kinetic energy spectra. They were associated with the familiar internal wave intermittency in the time domain ($\sim$10 waves in a group) and evidence of interaction between principal frequencies f and tidal constituents (N_2, M_2, S_2; below, these three frequencies are represented by m_2) with dominant subinertial motions varying with typical periods of O(100 days) (Figure 2). Such interactions generated motions at frequencies like 0.99f, 1.01f, and $0.99m_2$, $1.01m_2$ filling both the near-inertial and the D_2-band in kinetic energy spectra, for example, $0.99N_2 - 1.01S_2 = 0.15$ cpd (H. van Haren, Incoherent internal tidal currents in the deep-ocean, submitted to *Ocean Dynamics*, 2003). This may explain the non-random, highly elevated, character of the nearly raw spectra in and around these bands (Figure 4). Although general polarization changes were found in larger bands of $\sim$0.9 cpd wide, they were evidence of the same interactions continuing further until about (1 ± 0.15)f, $(1 \pm 0.15)m_2$, filling the entire fSD band (Figure 4; $1.15f = 1.67$ cpd, $0.85M_2 = 1.64$ cpd). Thus the width of the polarization bands was determined by the extent in frequency of subinertial motions. Although motions at frequencies farther from peak frequencies were less energetic, their polarization was the same (Figure 4). As a result, such motions were not random noise, and random statistics may not be applicable, as for pure deterministic signals.

[22] Broadening of the inertial peak could also result from changes in low-frequency vorticity $\zeta = \partial[v]/\partial x - \partial[u]/\partial y$, brackets denoting daily averaging, as the effective local inertial frequency is defined as $f_{eff} = f + 0.5\zeta$ [*Mooers*, 1975; *Kunze*, 1985]. However, this does not explain broadening of m_2 (by the same amount) without considering the above iterations.

[23] The suggested importance of internal wave groups for the entire internal wave band and their interaction with the varying background requires further investigation, especially the influence of internal wave groups on internal wave mixing as advocated by *Shrira* [1981] and *Thorpe* [1999]. The observed details in our spectra and suggested influence of internal wave groups may be just typical for the area of investigation (the continental slope), as the spectra seemed less continuous than those observed by *Müller et al.* [1978]. On the other hand, lack of spectral details may partly be due to smoothing, as indications of similar spectral structure as observed here, like higher harmonics $M_2 + f$ and M_4, were visible in some of *Fu*'s [1981] spectra.

6. Conclusions

[24] Rotary spectra were analyzed using 11 months of current meter data down the continental slope of the Bay of Biscay. Rotary spectral properties emphasized previous findings concerning kinetic energy spectra. It was found that:

[25] 1. Rotary coefficient (equation (6)) and rotary amplitude ratios (equation (9)) were characterized by a series of bands of peaks separated by intervening bands with low values. These bands had a near constant width in frequency $\Delta\sigma = 0.9 \pm 0.1$ cpd.

[26] 2. The width of these bands manifested nonlinear interactions between subinertial (dominant around $\sim$0.01 cpd) and near-inertial and tidal motions.

[27] 3. Depending on the relative strength of near-inertial motions compared with tidal motions, the above peaks were centered around (relatively high-energetic) sum-xinertial-tidal or even tidal-tidal nonlinear interaction frequencies.

[28] 4. These peaks best satisfied what was previously called "linear wave" theory and which implied symmetric nonlinear forcing generating dominantly clockwise polarization.

[29] 5. While at the frequencies of the above gaps, centered around (relatively low-energetic) difference inertial-tidal interaction frequencies, nearly rectilinear motions were found due to asymmetric "forcing." The main conclusion was that rotary spectral properties were useful to show the importance of nonlinear forcing of higher frequency internal waves, not attributable to fine-structure contamination.

[30] **Acknowledgments.** I enjoyed the assistance of the crew of the R/V *Pelagia* during deployment and recovery of all moorings. Margriet Hiehle designed Figure 1. I thank Hendrik van Aken for the use of current meter data from his "TripleB" project in the Bay of Biscay, which was supported by a grant from the Netherlands organization for the advancement of scientific research, NWO. Royal Netherlands Institute for Sea Research contribution number 3643.

References

Alford, M. H., Fine-structure contamination: Observations and a model of a simple two-wave case, *J. Phys. Oceanogr.*, *31*, 2645–2649, 2001.

Ekman, V. W., On the influence of the Earth's rotation on ocean currents, *Arch. Math., Astron. Phys.*, *2*(11), 1–53, 1905.

Fu, L.-L., Observations and models of inertial waves in the deep ocean, *Rev. Geophys.*, *19*, 141–170, 1981.

Garrett, C. J. R., and W. H. Munk, Space-time scales of internal waves, *Geophys. Fluid Dyn.*, *3*, 225–264, 1972.

Gonella, J., A rotary-component method for analysing meteorological and oceanographic vector time series, *Deep Sea Res.*, *19*, 833–846, 1972.

Kunze, E., Near-inertial wave propagation in geostrophic shear, *J. Phys. Oceanogr.*, *15*, 544–565, 1985.

LeBlond, P. H., and L. A. Mysak, *Waves in the Ocean*, 602 pp., Elsevier Sci., New York, 1978.

Mihaly, S. F., R. E. Thomson, and A. B. Rabinovich, Evidence for nonlinear interaction between internal waves of inertial and semidiurnal frequency, *Geophys. Res. Lett.*, *25*(8), 1205–1208, 1998.

Mooers, C. N. K., Several effects of a baroclinic current on the cross-stream propagation of inertial-internal waves, *Geophys. Fluid Dyn.*, *6*, 245–275, 1975.

Müller, P., D. J. Olbers, and J. Willebrand, The Iwex spectrum, *J. Geophys. Res.*, *83*, 479–500, 1978.

Müller, P., G. Holloway, F. Henyey, and N. Pomphrey, Non-linear interactions among internal gravity waves, *Rev. Geophys.*, *24*, 493–536, 1986.

Phillips, O. M., *The Dynamics of the Upper Ocean* (2nd ed.), 336 pp., Cambridge Univ. Press, New York, 1977.

Shrira, V. I., On the propagation of a three-dimensional packet of weakly non-linear internal gravity waves, *Int. J. Non-Lin. Mech.*, *16*, 129–138, 1981.

Thorpe, S. A., On internal wave groups, *J. Phys Oceanogr.*, *29*, 1085–1095, 1999.

van Haren, H., L. Maas, J. T. F. Zimmerman, H. Ridderinkhof, and H. Malschaert, Strong inertial currents and marginal internal wave stability in the central North Sea, *Geophys. Res. Lett.*, *26*(19), 2993–2996, 1999.

van Haren, H., L. Maas, and H. van Aken, On the nature of internal wave spectra near a continental slope, *Geophys. Res. Lett.*, *29*(12), 1615, doi:10.1029/2001GL014341, 2002.

Xing, J., and A. M. Davies, Processes influencing the nonlinear interaction between inertial oscillations, near inertial internal waves and internal tides, *Geophys. Res. Lett.*, *29*(5), 1067, doi:10.1029/2001GL014199, 2002.

H. van Haren, Royal Netherlands Institute for Sea Research (NIOZ), P.O. Box 59, NL-1790 AB Den Burg, Netherlands. (hansvh@nioz.nl)